ChemPubSoc Europe

DOI: 10.1002/cctc.201402124

Stereo- and Chemoselective Character of Supported CeO_2 Catalysts for Continuous-Flow Three-Phase Alkyne Hydrogenation

Gianvito Vilé,[a] Sabine Wrabetz,[b] Leonard Floryan,[a] Manfred Erwin Schuster,[b] Frank Girgsdies,[b] Detre Teschner,[b] and Javier Pérez-Ramírez*[a]

TiO_2-, Al_2O_3-, and ZrO_2-supported CeO_2 catalysts with different Ce loadings were prepared by wet impregnation of the carriers with an acidified solution of cerium ammonium nitrate. The calcined catalysts were characterized by bulk and surface-sensitive techniques, which included microcalorimetry, and evaluated in the three-phase hydrogenation of alkynes under continuous-flow conditions at variable temperature (293–413 K) and pressure (1–90 bar). A number of acetylenic compounds, which contain terminal or internal triple bonds, conjugated unsaturations, and additional functionalities, were systematically assessed. The results revealed the full stereo- and chemoselective character of the ceria catalysts, which outperform the well-known Lindlar catalyst, and open promising perspectives for the revolutionary use of a cost-effective oxide for the production of olefinic compounds in the vitamin and fine chemical industries.

Introduction

As one of the most intriguing oxides,[1] ceria is used as a support, stabilizer, promoter, or catalyst in a wide range of applications, which include the purification of exhaust automotive gases in three-way catalytic converters, the production of hydrogen in low-temperature solid oxide fuel cells, the preferential oxidation of CO in hydrogen-rich steams, and the recycling of chlorine by the catalyzed HCl oxidation.[2] This is because of the unique structural and electronic properties of ceria, associated with its ability to switch quickly between the Ce^{4+} and Ce^{3+} oxidation states, forming and annihilating oxygen vacancies in a stable fluorite-type structure.[3]

The discovery that pure CeO_2 catalyzes the gas-phase semihydrogenation of acetylene and propyne to the corresponding olefins has recently broadened the scope of ceria in catalysis.[4] These reactions, which are performed over Pd catalysts, are crucial steps for the purification of olefin streams in the petrochemical industry.[5] A CeO_2 catalyst with high surface area and no oxygen vacancies is beneficial to attain high olefin selectivities (86% to ethylene and 91% to propene in the hydrogenation of acetylene and propyne, respectively).[4a] Additionally, a large hydrogen excess in the feed mixture and temperatures above 473 K are required in the reaction, which suggests that hydrogen splitting is the rate-limiting step. DFT calculations on CeO_2(111) have provided an understanding of the ceria-catalyzed acetylene hydrogenation mechanism.[4b] Particularly, the function of ceria in the activation of hydrogen and stabilization of reactive radical species, the large energy barriers for the over-hydrogenation steps, and the isolation of the active site that inhibits the oligomerization pathways explain the high olefin yields obtained.

On the basis of these results, it is appropriate to assess the performance of ceria in the three-phase (liquid–gas–solid) hydrogenation of acetylenic compounds, if we consider the importance of the latter reaction for the synthesis of *cis*-alkenes, essential building blocks for fine chemicals and pharmaceuticals.[6] So far, the application of CeO_2 in liquid-phase hydrogenation is limited to the reduction of nitroarenes and carboxylic acids.[7] Besides, it is important to optimize the utilization of the ceria phase by its deposition on a suitable carrier. Herein, supported CeO_2 catalysts have been prepared, characterized, and evaluated in the three-phase hydrogenation of different acetylenic compounds at variable temperature (293–413 K) and pressure (1–90 bar). All catalytic tests were conducted under continuous-mode operation. In contrast to batch and semibatch setups, which are commonly employed for laboratory testing, continuous-flow hydrogenation reactors can be operated efficiently at steady state and offer key advantages for sustainable production in the pharmaceutical and fine chemical industries, such as cost reduction, efficient heat transfer, rapid mixing, small volume usage, and the capability for process integration and intensification.[8] The outstanding stereo- and chemoselective character of CeO_2, which exceeds that of the conventional Lindlar catalyst (Pb-poisoned Pd supported on calcium carbonate),[9] offers interesting perspectives for the

[a] G. Vilé, L. Floryan, Prof. J. Pérez-Ramírez
Institute for Chemical and Bioengineering
Department of Chemistry and Applied Biosciences
ETH Zurich
Vladimir-Prelog-Weg 1, CH-8093 Zurich (Switzerland)
E-mail: jpr@chem.ethz.ch

[b] Dr. S. Wrabetz, Dr. M. E. Schuster, Dr. F. Girgsdies, Dr. D. Teschner
Fritz-Haber-Institute of the Max Planck Society
Faradayweg 4-6, 14159 Berlin (Germany)

Supporting information for this article is available on the WWW under http://dx.doi.org/10.1002/cctc.201402124.

use of this metal oxide in the liquid-phase hydrogenation of alkynes.

Results and Discussion

Catalyst preparation and characterization

The supported ceria catalysts were prepared by wet impregnation of TiO_2, Al_2O_3, and ZrO_2 with a 9 M HNO_3 aqueous solution of cerium ammonium nitrate. Particularly, it has been shown that the use of an acidic medium during the impregnation enhances the dispersion of the ceria phase to provide the supported catalysts with relatively small CeO_2 nanoparticles.[10] The BET surface area of the supports was retained upon incorporation of the CeO_2 phase (Table 1). Inductively coupled plasma optical emission spectroscopy (ICP-OES) confirmed that the actual Ce loading is close to its nominal value (Table 1), and X-ray fluorescence (XRF) verified the absence of traces of typical hydrogenation metals in any of the samples.

The size and distribution of the CeO_2 nanoparticles were characterized by different techniques (Figures 1–3). High-resolution transmission electron microscopy (HRTEM) analysis of the 20 wt% CeO_2/TiO_2 catalyst (Figure 1a) revealed the presence of CeO_2 particles in the range of 5–10 nm supported on TiO_2 particles of approximately 15 nm.

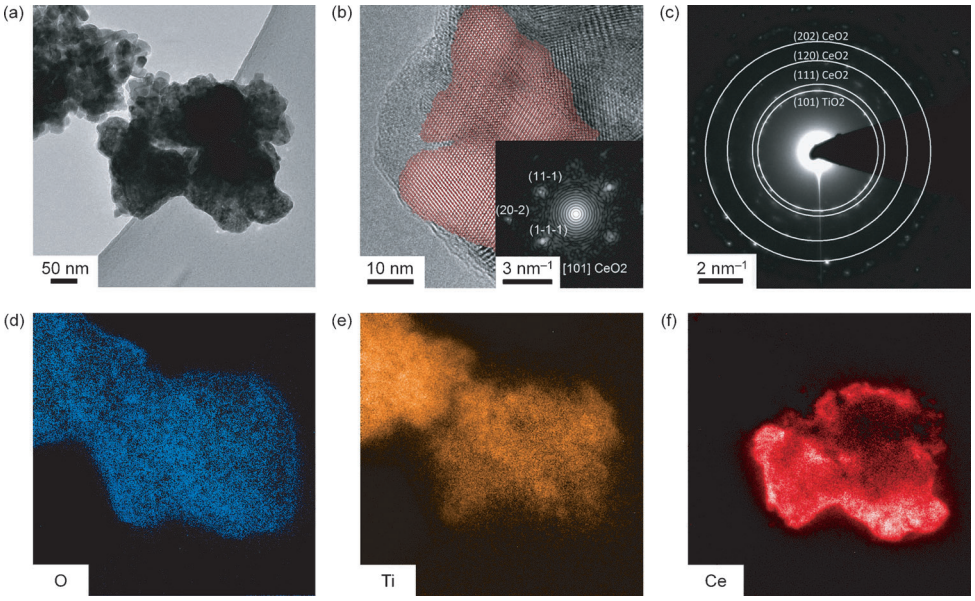

Figure 1. HRTEM images of 20 wt% CeO_2/TiO_2 in a region of the catalyst with a high Ce content. a) Low- and b) high-magnification micrographs and c) diffraction pattern of the agglomerate shown in a). EFTEM maps of d) O, e) Ti, and f) Ce that correspond to micrograph a).

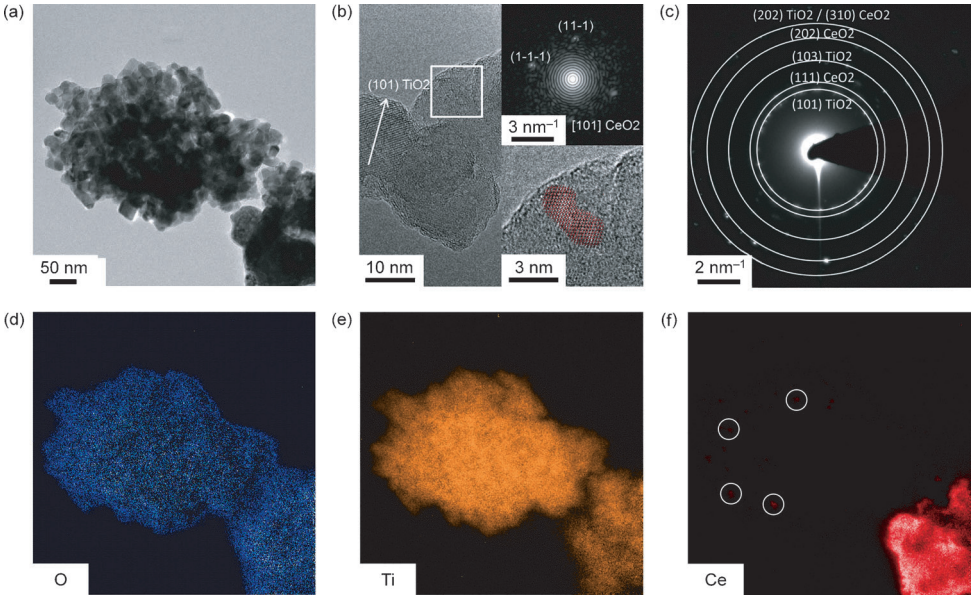

Figure 2. HRTEM images of 20 wt% CeO_2/TiO_2 in a region of the catalyst with a low Ce content. a) Low- and b) high-magnification micrographs and c) diffraction pattern of the agglomerate shown in a). EFTEM maps of d) O, e) Ti, and f) Ce that correspond to micrograph a).

Table 1. Characterization and catalytic data of ceria-based catalysts.

Catalyst	Ce content[a] [wt%]	S_{BET} [$m^2\ g^{-1}$]	a_{CeO_2}[b] [Å]	Acetylene hydrogenation[c]		1-Hexyne hydrogenation[d]	
				$X(C_2H_2)$ [%]	$S(C_2H_4)$ [%]	$X(C_6H_{10})$ [%]	$S(C_6H_{12})$ [%]
5 wt% CeO_2/TiO_2	4.2	52 (49)[e]	–	14	88	46	100
10 wt% CeO_2/TiO_2	8.0	51	–	25	89	68	100
20 wt% CeO_2/TiO_2	16.2	54	5.394 ± 0.004, 5.416 ± 0.002	54	90	90	100
20 wt% CeO_2/Al_2O_3	16.2	226 (242)	5.413 ± 0.002	51	87	87	89
20 wt% CeO_2/ZrO_2	16.0	45 (47)	–	53	89	87	100

[a] Determined by ICP-OES. [b] Determined by XRD. [c] Conditions: $W_{cat} = 0.56$ g, $T = 523$ K, $P = 1$ bar, $H_2/C_2H_2 = 30$, $F_G = 6$ $cm^3\ min^{-1}$. [d] Conditions: $W_{cat} = 0.85$ g, $T = 413$ K, $P = 90$ bar, F_L(solvent+substrate) = 0.3 $cm^3\ min^{-1}$, $F_G(H_2) = 60$ $cm^3\ min^{-1}$. [e] BET surface area of the pure support in brackets.

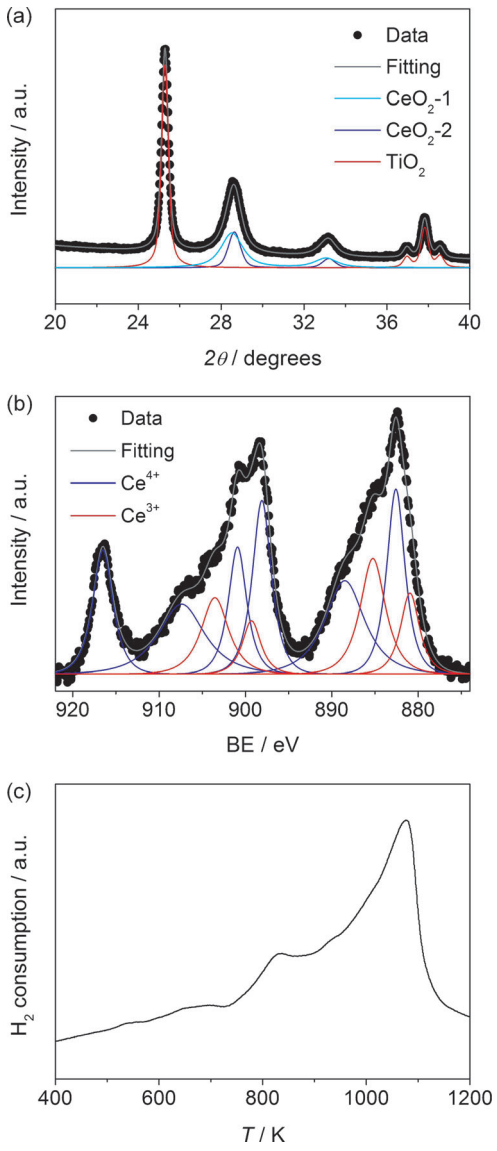

Figure 3. a) XRD pattern fitted with the TiO_2 and CeO_2 phases, b) Ce 3d core-level XPS spectrum fitted with Ce^{3+} and Ce^{4+} peaks, and c) H_2-TPR of 20 wt% CeO_2/TiO_2.

The ceria phase is accumulated mostly in a specific region, which is shown in red in Figure 1b. The diffraction pattern that corresponds to the whole catalyst agglomerate with the characteristic lattice planes of TiO_2(1 0 1) and CeO_2(1 1 1), (1 2 0), and (2 0 2) is depicted in Figure 1c. The energy-filtered transmission electron microscopy (EFTEM) maps of the micrograph shown in Figure 1a for O, Ti, and Ce are presented in Figure 1d–f, which suggest that Ce is mainly present in the central part of the agglomerate and is absent in the upper left corner. The whole upper agglomerate of Figure 1a is presented in Figure 2a, and Figure 2b shows a portion of it in which mostly anatase TiO_2 can be found. Nevertheless, the elongated crystalline particle in the white square (enlarged, filtered, and colored in red in the lower inset) can be assigned to CeO_2 as shown clearly by the corresponding fast Fourier transform (FFT) pattern displayed in Figure 2b and c. EFTEM analysis (Figure 2d–f) of the region shown in Figure 2a suggests that Ce is nearly absent, and the few CeO_2 particles are circled in white (Figure 2f). Hence, microscopy indicates that the overall distribution of Ce within the sample is heterogeneous, but the ceria particles found are nevertheless small.

X-ray diffraction (XRD) analysis of the same catalyst (Figure 3a) confirms that the support phase is solely anatase and indicates the formation of CeO_2 with a face-centered cubic fluorite structure with an average ceria crystallite size of 7.5 ± 0.2 nm. The contribution to the ceria peaks shows a slight asymmetry, which would not be expected in the case of peak broadening caused exclusively by the crystallite size and microstrain effects. Hence, a second ceria phase was introduced in the fit, with peak shape and lattice parameters refined independently from the first phase. The result looks consistently better over the whole angular range, which demonstrates that the qualitative nature of the peak asymmetry is the same for all of the ceria peaks. This result should not be considered in the sense of two distinct ceria phases that coexist in the sample; instead, it suggests a heterogeneous distribution of lattice parameters in the ceria phase. The integral near-surface composition has been examined by X-ray photoelectron spectroscopy (XPS), and the Ce/Ti ratio is 0.22, which confirms that ceria does not likely form large particles. The surface of ceria is partially reduced (28% Ce^{3+}), as observed by fitting the Ce 3d core-level spectrum (Figure 3b). The complex Ce 3d structure of cerium oxide arises from the various possible final states of the O-Ce charge transfer. The reducibility of 20 wt% CeO_2/TiO_2 has been further investigated by H_2 temperature-programmed reduction (TPR), and the profile shown in Figure 3c shows an H_2 uptake that increases slowly from 400–900 K, which corresponds to surface reduction and slow vacancy transport to the subsurface, and a main peak around 1100 K caused by the reduction of the bulk of the CeO_2 particles.

Alkyne hydrogenation

The results summarized in Table 1 for the hydrogenation of acetylene and 1-hexyne over different CeO_2-based catalysts show that the alkyne conversion increases with an increased Ce content and is not influenced by the type of support. The latter can be explained by the equivalent characterization results obtained over 20 wt% CeO_2/Al_2O_3 (Figure S1) and 20 wt% CeO_2/TiO_2. In any case, the olefin selectivity is constant at 90% in the gas-phase semi-hydrogenation of acetylene and 100% in the three-phase semi-hydrogenation of 1-hexyne. The performance of the 20 wt% CeO_2/TiO_2 catalyst in the hydrogenation of 1-hexyne has been further investigated at various conditions of temperature and pressure (Figure 4a). A high degree of alkyne conversion (>80%) is obtained only for $T > 400$ K and $P > 50$ bar. However, at each condition of temperature and pressure, the selectivity to 1-hexene is 100%. The catalyst stability has been verified additionally in a catalytic run with an extended period of time (Figure 4b). No decrease in alkyne conversion and alkene selectivity was detected during 8 h on stream. The hydrogenation performance of supported ceria in the presence and absence of 1-hexene in the reaction feed is

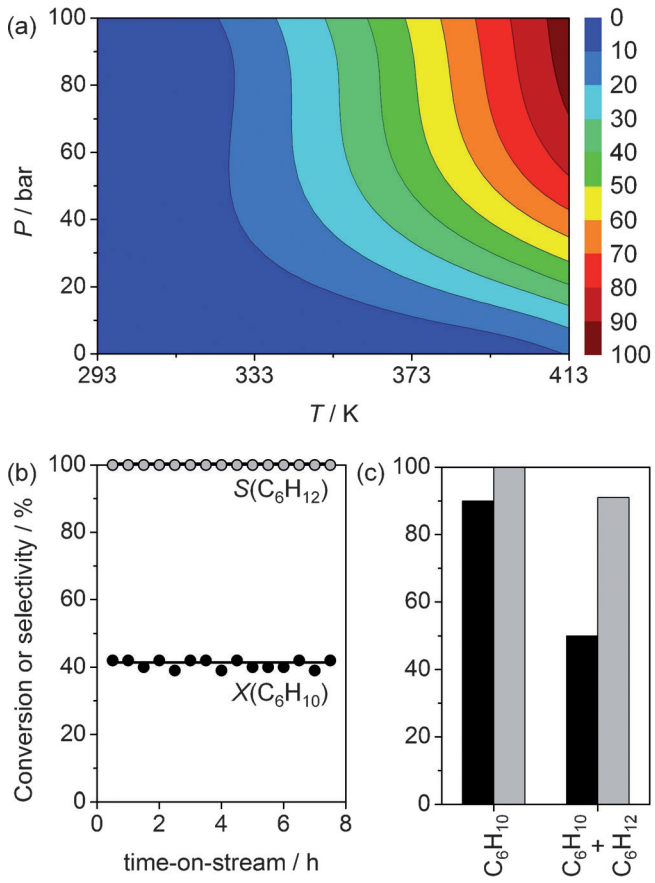

Figure 4. a) Influence of the temperature and pressure on the hydrogenation of 1-hexyne over 20 wt% CeO_2/TiO_2; the scale bar represents the alkyne conversion. B) Conversion of 1-hexyne and selectivity to 1-hexene over 20 wt% CeO_2/TiO_2 versus time-on-stream at $T=413$ K and $P=20$ bar. c) Performance of 20 wt% CeO_2/TiO_2 in 1-hexyne hydrogenation at $T=413$ K and $P=90$ bar in the absence and presence of 1-hexene in the reaction feed (1-hexyne:1-hexene = 1:1). Other reaction conditions: $W_{cat}=0.85$ g, F_L(solvent+substrate) = 0.3 $cm^3 min^{-1}$, $F_G(H_2)=60$ $cm^3 min^{-1}$.

depicted in Figure 4c. Compared to the hydrogenation of 1-hexyne (90% alkyne conversion and full olefin selectivity), a significant decrease in alkyne conversion (down to 50%) is observed for the hydrogenation of 1-hexyne+1-hexene, which indicates that alkynes and alkenes compete for adsorption. Despite the minute amount of *n*-hexane formed, the partial hydrogenation of 1-hexyne to 1-hexene is still by far the dominant reaction.

To correlate the catalytic performance with the characteristic properties of ceria, the chemisorption of 1-hexyne was further studied by microcalorimetry (Figure 5). As the Arrhenius plot of 1-hexyne hydrogenation was linear in the whole 353–413 K range, 1-hexyne adsorption was investigated at 353 K. The differential heat of adsorption profile as a function of 1-hexyne uptake reveals a very strong irreversible adsorption at the initial stage (up to 900 kJ mol^{-1}), which suggests that multiple dehydrogenation steps take place. After approximately 0.01 mmol g^{-1} 1-hexyne uptake, the heat of adsorption stabilizes at around 200 kJ mol^{-1} with a subsequent 0.06 mmol g^{-1} adsorption. This heat of adsorption resembles the energy released upon a single dehydrogenation step of acetylene.[4b]

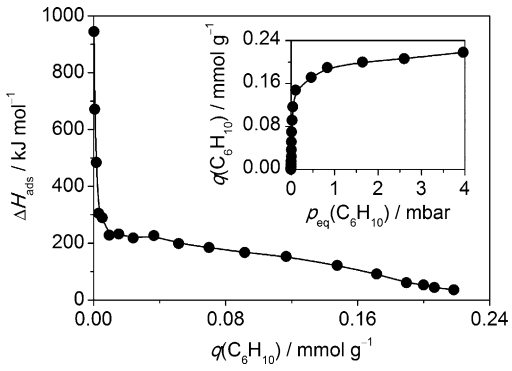

Figure 5. Differential heat of adsorption of 1-hexyne over 20 wt% CeO_2/TiO_2. The inset shows the relative adsorption isotherm at 353 K.

Further adsorption takes place with heat evolution that decreases slowly to 0.22 mmol g^{-1}, after which only physisorption occurs. These results indicate that, under the reaction conditions, a significant portion of the surface sites is covered by dehydrogenated species, not being available for hydrogenation. This is in line with DFT calculations of acetylene adsorption on CeO_2(111) that show that the most preferred adsorption mode is dissociative with respect to the C–H bond.[4b] 1-Hexyne and 1-hexene can compete for the remaining surface sites, in agreement with our catalytic data, but the negligible selectivity for full hydrogenation corroborates that the reduction of alkenes possesses a high energetic barrier.[4b]

The TiO_2-supported 20% wt% ceria catalyst has been tested over a broad range of acetylenic substrates, and the alkyne conversion and the product selectivity for each compound at fixed conditions of temperature, pressure, and flow rate are summarized in Table 2. The hydrogenation of 1-pentyne yields 55% alkyne conversion and 100% alkene selectivity. Under similar experimental conditions, a much higher alkyne conversion (90–94%) with full olefin selectivity is obtained for the hydrogenation of 1-hexyne and 1-decyne, which suggests that the reduction of higher alkynes on ceria present a lower energy barrier for the critical elementary steps and/or that there is a higher coverage of H species in this case. If the C≡C unsaturation is shifted from a terminal to an internal position, the hydrogenation of 2-pentyne (42% alkyne conversion and 100% alkene selectivity) and 3-hexyne (93% alkyne conversion and 100% alkene selectivity) produce only the *cis*-alkene isomer, which proves that *cis*/*trans* isomerization is impeded on ceria. In the hydrogenation of alkynes that contain multiple unsaturations, full selectivity to the double bond at a degree of alkyne conversion of 31 and 100% is achieved for the hydrogenation of 1-penten-4-yne and phenylacetylene, respectively, over 20 wt% CeO_2/TiO_2. The lower conversion for 1-penten-4-yne can be ascribed to competitive adsorption of the double bond unsaturation (vide supra). Finally, if we consider multifunctionalized substrates, the hydrogenation of 3-methyl-1-pentyn-3-ol (53% conversion and 95% selectivity to 3-methyl-1-penten-3-ol), 9-hexadecyn-1-ol (58% conversion and 100% selectivity to *cis*-9-hexadecen-1-ol), 1,1-diphenyl-prop-2-yn-1-ol (51% conversion and 100% selectivity to 1,1-di-

Table 2. Semi-hydrogenation of acetylenic compounds over the 20 wt% CeO_2/TiO_2 and Pd-Pb/$CaCO_3$ catalysts.

Substrate	Desired product	20 wt% CeO_2/TiO_2 Conversion[a] [%]	20 wt% CeO_2/TiO_2 Selectivity[a] [%]	Pd-Pb/$CaCO_3$ Conversion[b] [%]	Pd-Pb/$CaCO_3$ Selectivity[a] [%]
 1-pentyne	 1-pentene	55	100	26	98 (93)[c]
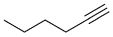 1-hexyne	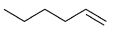 1-hexene	90	100	31	98 (94)
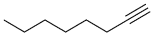 1-decyne	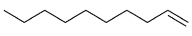 1-decene	94	100	not performed	
 2-pentyne	 *cis*-2-pentene	42	100	27	96 (93)
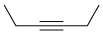 3-hexyne	 3-hexene	93	100	32	100 (94)
 1-penten-4-yne	 1,4-pentadiene	31	100	not performed	
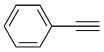 phenylacetylene	 styrene	100	100	29	98 (91)
 3-methyl-1-pentyn-3-ol	 3-methyl-1-penten-3-ol	53	95[d]	27	83 (78)
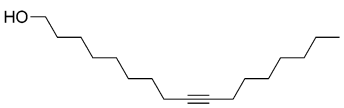 9-hexadecyn-1-ol	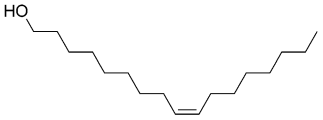 *cis*-9-hexadecen-1-ol	58	100	34	86
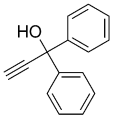 1,1-diphenylprop-2-yn-1-ol	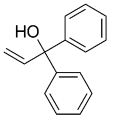 1,1-diphenylprop-2-en-1-ol	51	100	35	100
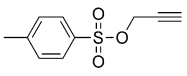 3-butynyl-*p*-toluenesulfonate	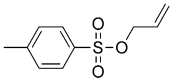 3-butenyl-*p*-toluenesulfonate	18	100	26	100 (93)

[a] Reaction conditions: $W_{cat} = 0.85$ g, $T = 413$ K, $P = 90$ bar, F_L(solvent+substrate) = 0.3 $cm^3 min^{-1}$, $F_G(H_2) = 60$ $cm^3 min^{-1}$. [b] Reaction conditions: $W_{cat} = 0.1$ g, $T = 293$ K, $P = 1$ bar, F_L(solvent+substrate) = 3 $cm^3 min^{-1}$, $F_G(H_2) = 18$ $cm^3 min^{-1}$. [c] Selectivity to the desired product at a conversion level matching that of the supported CeO_2 catalyst is given in brackets. Reaction conditions: $W_{cat} = 0.1$ g, $T = 293$ K, $P = 1$ bar, F_L(solvent+substrate) = 0.3–3 $cm^3 min^{-1}$, $F_G(H_2) = 1.8$–18 $cm^3 min^{-1}$. [d] The selectivity to 2-methyl-3-butan-2-ol was 5%.

phenylprop-2-en-1-ol), and 3-butynyl-*p*-toluenesulfonate (18% conversion and 100% selectivity to the respective alkene) occur both stereo- and chemoselectively as the hydroxyl and sulfonate functionalities are intact. Except for the hydrogenation of 3-methyl-1-pentyn-3-ol, producing 5% selectivity to 3-methyl-pentan-3-ol, in all of the other cases, saturated compounds and oligomers were not detected. Potentially, the absence of green oil might be because of the dilute 1 vol% alkyne solution and, consequently, the low concentration of oligomers. Therefore, we conducted the solvent-free hydrogenation of 1-hexyne over 20 wt% CeO_2/TiO_2 under the conditions indicated in Table 2. Also in this case, the carbon balance was close to 100 ± 3% and the reaction was fully selective to the alkene.

The reactions proceed in all cases with full selectivity to the olefin. These results exceed the performance of the archetypal Lindlar catalyst, which was assessed at a low and high degree of alkyne conversion and displayed an excellent but somewhat lower degree of alkene selectivity (Table 2). The excellent stereo- and chemoselectivity of supported ceria is tentatively assigned to the isolation of the active sites,[4b] which prevent the reorganization and *cis*/*trans* isomerization of the adsorbed alkene species, similarly to the stereo- and chemoselective hydrogenation of acetylenic compounds over Pb-poisoned and ligand-modified Pd nanoparticles.[11] Despite the demanding temperature and pressure conditions of CeO_2, the doping of CeO_2 with different types of cations as well as the preparation of ceria catalysts with distinct morphologies, which are effi-

cient and versatile ways to modulate the chemical properties of CeO_2,[12] might enhance the reactivity of ceria, allowing operation at milder conditions.

Finally, the quantitative rationalization of the influence of the ceria loading on the TiO_2-supported catalysts remains an open aspect at this stage. No reflections associated with CeO_2 were observed in the XRD patterns of the 5 and 10 wt% CeO_2/TiO_2 samples, which indicates the very high dispersion of the ceria phase on the titania carrier. XPS measurements show that the surface concentration of Ce^{3+} increases linearly with the decreased ceria loading (Figure S2). A higher amount of oxygen vacancies is detrimental for the alkyne hydrogenation activity.[4a] However, the overall reaction rate should be determined by the interplay between dispersion (a priori beneficial, higher at a low CeO_2 loading) and degree of surface reduction (detrimental, higher at a low CeO_2 loading). The reaction rate in acetylene hydrogenation per mole of total ceria is very similar over 5 and 20 wt% CeO_2/TiO_2, which suggests that the benefits derived from the higher dispersion of active phase in the former catalyst are offset by the higher degree of ceria reduction in the smaller particles. For the hexyne hydrogenation, the rate was two times higher over 5 wt% CeO_2/TiO_2, which suggests the occurrence of less surface reduction in liquid-phase operation. The above discussion is speculative but it reflects the complexity related to the amount and type of exposed Ce sites and calls for extensive studies to unravel detailed structure–performance relationships for these catalysts for gas- and liquid-phase hydrogenation.

Conclusions

We have demonstrated the highly selective character of supported CeO_2 catalysts in the semi-hydrogenation of alkynes. The materials were prepared by simple impregnation of the supports with a Ce salt in an acidic medium, and the selectivity to the alkene was not affected by the type of carrier and the Ce loading. The ethylene selectivity in the gas-phase hydrogenation of acetylene reached 90%, and the results for the three-phase hydrogenation under flow conditions were even more impressive: full stereo- and chemoselectivity to the *cis*-alkene was attained over a wide range of acetylenic substrates, that is, oligomers and overhydrogenated products were not observed, and the performance was stable for several hours on stream. The CeO_2-based catalysts required demanding conditions of temperature and pressure (413 K, 90 bar) because of the intrinsic inability of ceria to activate hydrogen. However, selectivity-wise, supported ceria outperformed the state-of-the-art Lindlar catalyst. Consequently, these results enable the use of a cheap metal oxide for the production of olefinic compounds in fine chemical and pharmaceutical applications.

Experimental Section

Catalyst preparation

Prior to use, TiO_2-anatase (Sigma–Aldrich, 99.7%), Al_2O_3 (Saint-Gobain NorPro, > 99.5%), and ZrO_2 (Saint-Gobain NorPro, > 99.8%) were calcined in static air at 773 K for 4 h (heating rate = 5 K min^{-1}). Wet impregnation of the support (1 g) was performed using 9 M HNO_3 aqueous solution of cerium ammonium nitrate (2.0 cm^3; Sigma–Aldrich, > 98%). The impregnated catalyst was collected by filtration, washed with deionized water, dried at 333 K for 12 h, and calcined in static air at 773 K for 4 h (heating rate = 5 K min^{-1}). The Lindlar catalyst evaluated in this study was provided by Alfa Aesar (ref: 043172) and contained 4.5 wt% Pd and 3.4 wt% Pb deposited on $CaCO_3$.

Catalyst characterization

The Ce content was determined by ICP-OES by using a Horiba Ultra 2 instrument after dissolution of the catalysts in a HF/HCl/HNO_3 solution. The absence of typical hydrogenation metals was verified by XRF by using an Orbis Micro-EDXRF analyzer, equipped with a 35 kV Rh anode and a silicon drift detector. N_2 sorption at 77 K was measured by using a Micromeritics Tristar II analyzer. Prior to the analysis, the samples were evacuated at 473 K for 10 h. TEM studies were performed by using an FEI Titan Cs 80–300 microscope equipped with a field-emission gun, a Gatan Tridiem filter, and an energy-dispersive X-ray (EDX) analyzer and operated at 300 keV. The samples were prepared by dry deposition onto a holey-carbon-covered Cu grid. The spherical aberration was corrected by using a CEOS Cs-corrector. HRTEM images were processed to obtain the power spectra, which were used to measure interplanar distances and angles for phase identification. For the EFTEM of O, Ti, and Ce, the O K edge at 530 eV, Ti L edge at 456 eV, and Ce N edge at 110 eV were analyzed. CeO_2 and TiO_2 phases were assigned according to ICSD number 246969 and 63711, respectively. The XRD measurement was performed by using a Bruker AXS D8 ADVANCE DAVINCI diffractometer equipped with a Ni filter and a LYNXEYE position sensitive detector ($CuK_{\alpha 1+2}$ radiation) in Bragg–Brentano geometry with a fixed divergence slit. The XRD data were analyzed by whole powder pattern fitting according to the Rietveld method by using the TOPAS software.[13a] Peak profiles were fitted by convolution of an instrumental contribution following the Fundamental Parameters approach,[13b] with a sample contribution based on the Double–Voigt approach.[13c] XPS was performed at RT by using non-monochromatized AlK_α (1486.6 eV) excitation and a hemispherical analyzer (Phoibos 150, SPECS). The sample mounted on conductive carbon tape was transferred to the spectrometer chamber under regular air exposure. The binding energy scale was calibrated by internal referencing to the Ce 3d U''' (916.7 eV) hybridization state of Ce^{4+} to correct for small charging effects. The Ce/Ti ratio of the sample was calculated from the Ce 3d and Ti 2p states after Shirley background subtraction by normalizing the peak areas with the corresponding cross sections, the transmission function of the lens system at the appropriate photoelectron kinetic energy, and with an inelastic mean free path correction to account for the different information depth of the Ce 3d and Ti 2p states. H_2-TPR was performed by using a Thermo TPD/R/O 1100 unit equipped with a thermal conductivity detector. The catalyst ($\approx$ 50 mg) was loaded in the quartz microreactor (11 mm i.d.), pretreated in He (20 cm^3 min^{-1}) at 473 K for 30 min, and cooled to 323 K in He. The analysis was performed in 5 vol% H_2/He (20 cm^3 min^{-1}), and the temperature was ramped from 323 to 1173 K at 5 K min^{-1}. Differential heats of adsorption were measured by using a SETARAM MS70 Calvet calorimeter. The calorimeter was combined with a custom-made high-vacuum and gas dosing apparatus described elsewhere.[13d] The sample was pretreated in O_2 at 523 K and 1 bar for 1 h. After evacuation, a second pretreatment in H_2 at 0.1 bar and 423 K for 1 h was performed to

mimic the reducing conditions under the hydrogenation reaction. The catalyst was finally degassed overnight. 1-Hexyne was stepwise introduced into the evacuated cell at 353 K, and the pressure evolution and heat signal were recorded for each dosing step. The adsorption isotherm was derived from the dosed amount and the equilibrium pressure, and the differential heats of adsorption were calculated by converting the thermal signal into heat by using the calorimeter's calibration factor and dividing the heat by the number of molecules adsorbed in the corresponding step.

Catalytic tests

The gas-phase hydrogenation of acetylene was performed by using a continuous-flow fixed-bed microreactor setup equipped with an on-line gas chromatograph.[5a] The testing conditions were as follows: $W_{cat} = 0.56$ g (particle size = 0.2–0.4 mm), $T = 523$ K, $p(C_2H_2) = 25$ mbar, $p(H_2) = 750$ mbar ($H_2/C_2H_2 = 30$), and $F_G = 6\ cm^3\ min^{-1}$. The three-phase hydrogenation of acetylenic compounds was performed by using a flooded-bed reactor (ThalesNano H-Cube Pro™), in which the liquid alkyne and the gaseous hydrogen flow concurrently upward through a fixed bed of catalyst particles.[11b] The reactor was equipped with a heating jacket and three thermocouples located at the inlet, in the center, and at the outlet of the catalyst bed. At steady state, the temperature difference between these thermocouples was less than 2 K, which ensured isothermal operation. Hydrogen was generated in situ by the electrolysis of millipore water and fed by a mass-flow controller. The liquid feed was supplied by a HPLC pump and mixed with the hydrogen before it entered the reaction chamber. The reactants included 1-pentyne (ABCR-Chemicals, 99%), 1-hexyne (Acros Organics, 98%), 1-decyne (TCI Deutschland, >95%), 2-pentyne (ABCR-Chemicals, 98%), 3-hexyne (TCI Deutschland, 98%), 1-hexene (Fluka-Chemie, >97%), 1-penten-4-yne (ABCR-Chemicals, 95%), phenylacetylene (Acros Organics, 98%), 3-methyl-1-pentyn-3-ol (TCI Deutschland, >98%), 9-hexadecyn-1-ol (ABCR-Chemicals, 97%), 1,1-diphenylprop-2-yn-1-ol (Sigma–Aldrich, 99%), and 3-butynyl-*p*-toluenesulfunate (TCI Deutschland, >95%). The catalyst (≈0.85 g for the ceria-based materials and ≈0.1 g for the Lindlar catalyst, particle size: 0.2–0.4 mm) was loaded into a cartridge of approximately 7 cm length × 0.35 cm internal diameter (volume of the catalyst bed = 0.67 cm^3). Reaction solutions contained 1 vol% of alkyne in solvent and, in case of mixtures, 1 vol% of alkyne and 1 vol% of alkene in solvent. Toluene (Acros Organics, 99.9%) was used as the solvent, and benzene (Sigma–Aldrich, >99.5%) was used as the internal standard. The three-phase hydrogenation tests were performed at different temperatures (293–413 K) and total pressures (1–90 bar), and the liquid (0.3 $cm^3\ min^{-1}$) and H_2 (60 $cm^3\ min^{-1}$) flow rates were kept constant. Under these conditions, the possibility of alkyne evaporation or leaching of the active phase could be excluded. The reaction products were collected at steady state, which was reached within 10 min, and analyzed offline by GC (HP 6890) equipped with a HP-5 capillary column and a flame ionization detector. In all cases, the conversion (X) of alkyne was determined as the amount of reacted alkyne divided by the amount of alkyne at the reactor inlet, whereas the selectivity (S) to a given compound was quantified as the amount of compound produced divided by the total amount of alkyne converted.

Keywords: alkynes · cerium · chemoselectivity · hydrogenation · supported catalysts

[1] C. T. Campbell, C. H. F. Peden, *Science* **2005**, *309*, 713.
[2] a) K. Otsuka, T. Ushiyama, I. Yamanaka, *Chem. Lett.* **1993**, *9*, 1517; b) A. Trovarelli, *Catal. Rev. Sci. Eng.* **1996**, *38*, 439; c) S. Park, J. M. Vohs, R. J. Gorte, *Nature* **2000**, *404*, 265; d) G. A. Deluga, J. R. Salge, L. D. Schmidt, X. E. Verykios, *Science* **2004**, *303*, 993; e) S. Carrettin, P. Concepción, A. Corma, J. M. López-Nieto, V. F. Puntes, *Angew. Chem. Int. Ed.* **2004**, *43*, 2538; *Angew. Chem.* **2004**, *116*, 2592; f) P. Concepción, A. Corma, J. Silvestre-Albero, V. Franco, J. Y. Chane-Ching, *J. Am. Chem. Soc.* **2004**, *126*, 5523; g) W. C. Chueh, Y. Hao, W. Jung, S. M. Haile, *Nat. Mater.* **2012**, *11*, 155; h) A. P. Amrute, C. Mondelli, M. Moser, G. Novell-Leruth, N. López, D. Rosenthal, R. Farra, M. E. Schuster, D. Teschner, T. Schmidt, J. Pérez-Ramírez, *J. Catal.* **2012**, *286*, 287.
[3] a) F. Esch, S. Fabris, L. Zhou, T. Montini, C. Africh, P. Fornasiero, G. Comelli, R. Rosei, *Science* **2005**, *309*, 752; b) S. Fabris, G. Vicario, G. Balducci, S. de Gironcoli, S. Baroni, *J. Phys. Chem. B* **2005**, *109*, 22860; c) M. V. Ganduglia-Pirovano, J. L. F. Da Silva, J. Sauer, *Phys. Rev. Lett.* **2009**, *102*, 026101; d) J.-F. Jerratsch, X. Shao, N. Nilius, H.-J. Freund, J. Sauer, *Phys. Rev. Lett.* **2011**, *106*, 246801.
[4] a) G. Vilé, B. Bridier, J. Wichert, J. Pérez-Ramírez, *Angew. Chem. Int. Ed.* **2012**, *51*, 8620; *Angew. Chem.* **2012**, *124*, 8748; b) J. Carrasco, G. Vilé, D. Fernández-Torre, R. Pérez, J. Pérez-Ramírez, M. V. Ganduglia-Pirovano, *J. Phys. Chem. C* **2014**, *118*, 5352.
[5] a) M. L. Derrien, *Stud. Surf. Sci. Catal.* **1986**, *27*, 613; b) A. Borodziński, G. C. Bond, *Catal. Rev. Sci. Eng.* **2006**, *48*, 91; c) F. Studt, F. Abild-Pedersen, T. Bligaard, R. Z. Sørensen, C. H. Christensen, J. K. Nørskov, *Science* **2008**, *320*, 1320; d) D. Teschner, J. Borsodi, A. Wootsch, Z. Révay, M. Hävecker, A. Knop-Gericke, S. D. Jackson, R. Schlögl, *Science* **2008**, *320*, 86; e) D. H. Mei, M. Neurock, C. M. Smith, *J. Catal.* **2009**, *268*, 181; f) M. Crespo-Quesada, A. Yarulin, M. Jin, Y. Xia, L. Kiwi-Misker, *J. Am. Chem. Soc.* **2011**, *133*, 12787.
[6] S. Nishimura, *Handbook of Heterogeneous Catalytic Hydrogenation for Organic Synthesis*, Wiley, New York, **2001**, p. 63.
[7] a) D. G. Cheng, M. Chong, F. Chen, X. Zhan, *Catal. Lett.* **2008**, *120*, 82; b) H.-Z. Zhu, Y.-M. Lu, F.-J. Fan, S.-H. Yu, *Nanoscale* **2013**, *5*, 72193.
[8] a) B. Gutmann, J.-P. Roduit, D. Roberge, C. O. Kappe, *Chem. Eur. J.* **2011**, *17*, 13146; b) M. Irfan, T. N. Glasnov, C. O. Kappe, *ChemSusChem* **2011**, *4*, 300; c) K. S. Elvira, X. Casadevall i Solvas, R. C. R. Wootton, A. J. deMello, *Nat. Chem.* **2013**, *5*, 905.
[9] H. Lindlar, *Helv. Chim. Acta* **1952**, *35*, 446.
[10] a) H. A. Larmie, US patent 5429647, **1995**; b) P. K. Rao, K. S. R. Rao, S. K. Masthan, K. V. Narayana, T. Rajiah, V. V. Rao, *Appl. Catal. A* **1997**, *163*, 123.
[11] a) M. García-Mota, J. Gómez-Díaz, G. Novell-Leruth, C. Vargas-Fuentes, L. Bellarosa, B. Bridier, J. Pérez-Ramírez, N. López, *Theor. Chem. Acc.* **2011**, *128*, 663; b) G. Vilé, N. Almora-Barrios, S. Mitchell, N. López, J. Pérez-Ramírez, *Chem. Eur. J.* **2014**, *20*, 5926 .
[12] a) S. Collins, G. Finos, R. Alcántara, E. Del Rio, S. Bernal, A. Bonivardi, *Appl. Catal. A* **2010**, *388*, 202; b) J. Vecchietti, S. Collins, W. Xu, L. Barrio, D. Stacchiola, M. Calatayud, F. Tielens, J. J. Delgado, A. Bonivardi, *J. Phys. Chem. C* **2013**, *117*, 8822; c) R. Farra, M. García-Melchor, M. Eichelbaum, M. Hashagen, W. Frandsen, J. Allan, F. Girgsdies, L. Szentmiklósi, N. López, D. Teschner, *ACS Catal.* **2013**, *3*, 2256; d) E. Aneggi, D. Wiater, C. de Leitenburg, J. Llorca, A. Trovarelli, *ACS Catal.* **2014**, *4*, 172.
[13] a) TOPAS, version 4.2, Bruker AXS, **2009**; b) R. W. Cheary, A. Coelho, *J. Appl. Crystallogr.* **1992**, *25*, 109; c) D. Balzar in *Defect and Microstructure Analysis from Diffraction* (Eds.: R. L. Snyder, H. J. Bunge, J. Fiala), International Union of Crystallography Monographs on Crystallography No. 10, Oxford University Press, New York, **1999**, pp. 94–126; d) L. C. Jozefowicz, H. G. Karge, E. N. Coker, *J. Phys. Chem.* **1994**, *98*, 8053.

Received: March 12, 2014
Published online on June 2, 2014